AD-A088 792 CORNELL UNIV ITHACA NY DEPT OF CHEMISTRY F/G 9/2
DIGITAL IMAGE PROCESSING IN ION MICROSCOPE ANALYSIS: METHODS OF--ETC(U)
AUG 80 D M DRUMMER, G H MORRISON N00014-80-C-0538
UNCLASSIFIED TR-2 NL

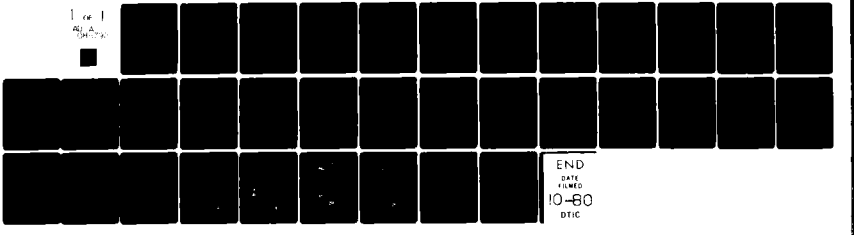

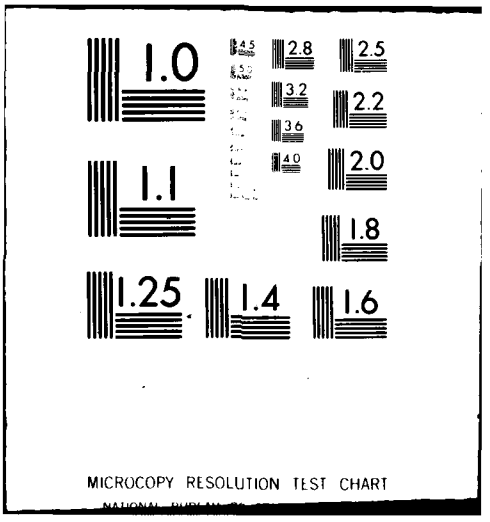
1.0
1.1
1.25
1.4
1.6
1.8
2.0
2.2
2.5
2.8
3.2
3.6
4.0
4.5
5.0
MICROCOPY RESOLUTION TEST CHART

AD A088792

OFFICE OF NAVAL RESEARCH

Contract N00014-80-C-0538

Task No. NR 051-736

TECHNICAL REPORT No. 2

Digital Image Processing in Ion Microscope Analysis:

Methods of Image Quantification,

by

D. M. Drummer and G.H. Morrison

Prepared for Publication

in

Analytical Chemistry

Cornell University
Department of Chemistry
Ithaca, N. Y. 14853

August 20, 1980

Reproduction in whole or in part is permitted for any purpose of the United States Government

This document has been approved for public release and sale; its distribution is unlimited

DDC FILE COPY

092619

80 8 22 029

SECURITY CLASSIFICATION OF THIS PAGE (When Data Entered)

REPORT DOCUMENTATION PAGE		READ INSTRUCTIONS BEFORE COMPLETING FORM
1. REPORT NUMBER: Technical Report No. 2 ✓	2. GOVT ACCESSION NO.: AD-A088 792	3. RECIPIENT'S CATALOG NUMBER
4. TITLE (and Subtitle): DIGITAL IMAGE PROCESSING IN ION MICROSCOPY: METHODS OF IMAGE QUANTIFICATION		5. TYPE OF REPORT & PERIOD COVERED: Interim Technical Report
		6. PERFORMING ORG. REPORT NUMBER
7. AUTHOR(s): D.M. DRUMMER AND G.H. MORRISON		8. CONTRACT OR GRANT NUMBER(s): ✓N00014-80-C-0538
9. PERFORMING ORGANIZATION NAME AND ADDRESS: Dept. of Chemistry ✓ Cornell University Ithaca, N. Y. 14853		10. PROGRAM ELEMENT, PROJECT, TASK AREA & WORK UNIT NUMBERS: NR051-736
11. CONTROLLING OFFICE NAME AND ADDRESS: ONR (472) 800 N. Quincy St., Arlington, VA 22217		12. REPORT DATE: August 20, 1980
		13. NUMBER OF PAGES: 34 pp.
14. MONITORING AGENCY NAME & ADDRESS (if different from Controlling Office)		15. SECURITY CLASS. (of this report): Unclassified
		15a. DECLASSIFICATION/DOWNGRADING SCHEDULE

16. DISTRIBUTION STATEMENT (of this Report)

Approved for public release: distribution unlimited

17. DISTRIBUTION STATEMENT (of the abstract entered in Block 20, if different from Report)

18. SUPPLEMENTARY NOTES

Prepared for publication in ANALYTICAL CHEMISTRY

19. KEY WORDS (Continue on reverse side if necessary and identify by block number)

Ion microscope, secondary ion mass spectrometry, digital image processing, ion implantation, imaging standards.

20. ABSTRACT (Continue on reverse side if necessary and identify by block number)

Two methods of secondary ion image quantification are applied to the analysis of a low-alloy steel, evaluated, and compared. The use of ion implantation for providing an internal standard element and for fabricating "imaging standards" for evaluation of quantification procedure accuracy is investigated and discussed. A basic philosophy is presented for multi-element, multi-feature analysis using ion images, and the use of effective display with the purpose of conveying meaningful compositional morphological information is investigated.

DD FORM 1 JAN 73 1473

SECURITY CLASSIFICATION OF THIS PAGE (When Data Entered)

DIGITAL IMAGE PROCESSING IN ION MICROSCOPE ANALYSIS: METHODS OF IMAGE QUANTIFICATION

D. M. Drummer and G. H. Morrison*

Department of Chemistry
Cornell University
Ithaca, N.Y. 14853

ABSTRACT: Two methods of secondary ion image quantification are applied to the analysis of a low-alloy steel, evaluated, and compared. The use of ion implantation for providing an internal standard element and for fabricating "imaging standards" for evaluation of quantification procedure accuracy is investigated and discussed. A basic philosophy is presented for multi-element, multi-feature analysis using ion images, and the use of effective display with the purpose of conveying meaningful compositional morphological information is investigated.

---

*Author to whom reprint requests should be addressed

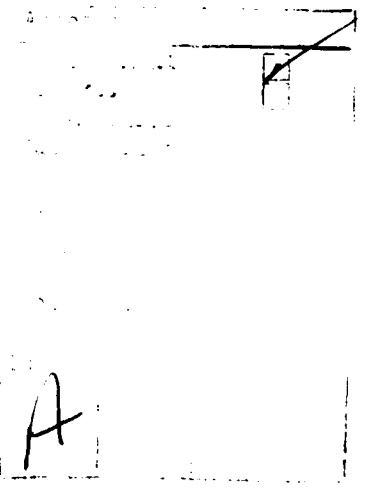

INTRODUCTION

The need to determine spatially resolved elemental distributions at the trace level is inherent in many problems of materials characterization. In many instances the properties of a material depend not only on the concentration of a trace constituent, but also on the distribution of that constituent on a microscale. The electron microprobe (1,2), ion microprobe (3,4), and scanning Auger microprobe (5,6) all have the proven capability to perform spatial compositional analysis and elemental imaging of the surface of a sample. In these cases the imaging process can be generalized as a sum of sequential point analyses with the probes operating in the scanning mode. In contrast, the ion microscope, a direct imaging ion microprobe, produces an elemental image of the sample surface by what can be described as simultaneous multipoint detection. The ion optics provide direct microscopic imaging by retaining a one-to-one correspondence between the point of origin of an ion emitted from the surface and its position in the final detected image. The resultant ion micrograph represents x-y elemental distributions, generally in the ppm range or lower, with a lateral resolution of about 1 micrometer. Direct imaging results in several advantages as compared to scanning microprobe imaging, including substantially decreased acquisition times, increased resolution, and often, increased precision, as the compromise between time and total number of counts recorded is usually eliminated. In addition, the imaging mode exploits the full potential of the ion microscope's ability to provide the spatial information which is often lost or severely compromised in a bulk or pseudo-imaging SIMS (Secondary Ion Mass Spectrometry) analysis.

Quantification of ion probe data has always been difficult due to serious matrix effects (7,8). In an ion microscope analysis, there exist other phenomena which induce artifical contrast into ion images, thus distorting the compositional information present. These include crystallographic, topographic, and chromatic contrast, as mentioned by Steiger and Rüdenauer (9). The result of these effects is that the transformation from an ion image to an elemental concentration map must be undertaken with a great deal of care and an understanding of the distortions present.

Despite the problems there have been many attempts to quantify non-imaging SIMS, with varying degrees of success. Two of the most popular methods have been empirical approaches such as the use of relative sensitivity factors (10), and the application of theoretical ionization models such as the Local Thermal Equilibrium (LTE) model originated by Andersen and Hinthorne (11). There have also been ion image quantification attempts, although they are much fewer in number. These include LTE type correction (9), sensitivity factor correction (12), and less complicated methods such as total current monitoring (13) and the application of simple correction factors (14).

Many of these methods apply the bulk-type correction schemes to an image by treating it as an assemblage of point analyses. At first glance this seems fairly straightforward, but in many cases approximations must be made to facilitate the correction. Most of these problems arise from the attempt to use bulk measurements to quantify a spatially resolved imaging analysis.

An example of this is any case where an internal standard is required. In a bulk analysis, it is sufficient to use a constituent which has been certified for bulk concentration by another analytical technique, but for a lateral analysis the concentration of the internal standard must be known at each discrete point of the resultant image. This restricts the selection either to an element with a well characterized heterogeneous distribution, or to

one that is homogeneous within the sample. The former of these criteria is very seldomly encountered, and even the latter may be unfeasible for many sample matrices.

In any sensitivity factor correction scheme it has usually been necessary to utilize a single set of sensitivity factors, even though within a given matrix an element having a constant concentration may exhibit a significant variation in detected signal relative to the reference element. This problem is described by Fassett and Morrison in their study of polycrystalline iron (15). The use of a constant set of sensitivity factors may therefore have a detrimental effect on the analytical results.

Another problem is how to evaluate the accuracy of a quantification scheme, as there currently exist no materials certified for heterogeneous trace element distributions on a microscale. In the past it has been most common practice either to integrate the corrected sample area back to a bulk concentration which is then compared to the known bulk concentration (9), or to evaluate accuracy in a qualitative fashion (14). Although this is helpful as a rough approximation of accuracy, it tends to be somewhat less than satisfying from an analytical viewpoint.

In this paper we consider the above mentioned problems; two approaches to ion image quantification are described. The first is a theoretical model correction of the 1-parameter LTE type requiring one internal standard, similar to that used by Steiger and Rüdenauer (9), but incorporating several modifications, as described below.

We utilize the LTE methodology only as a mathematical modelling approach which uses an exponential dependence of ionization fraction on ionization potential to effect corrections, and do not attempt to justify its corrections on a theoretical basis. An evaluation of several semi-theoretical models for

SIMS quantification has been published by Rudat and Morrison (16). The second is an application of the Matrix Ion Species Ratio method (MISR), a sensitivity factor approach by Gangei, et. al. (7), again with some modifications to facilitate its use with ion images. These two methods are applied to the analysis of a NBS low alloy steel reference material, evaluated, and compared.

In addition, we investigate the use of the ion implantation technique, which has been described in detail elsewhere (17,18). Ion implantation is used both as a means of providing an internal standard element in cases where one may not exist, and as a way to fabricate "image standards" for use as a means of testing the accuracy of a quantification method.

EXPERIMENTAL

Instrumentation. The CAMECA IMS-300 Ion Microscope used in these studies was developed by Castaing and Slodzian (19) and described in detail previously (10). The ion microscope is directly interfaced to a PDP 11/20 minicomputer with various storage and input/output devices, which allows data collection in the non-imaging mode. Ion images were recorded on electron sensitive film (Agfa Gevaert 37C50) and converted to digital form with a scanning microphotodensitometer (Photomation Mark II). A more detailed description of the hardware system, the densitometer, and the correction for nonlinear response of the film has been published previously (21).

An Accelerators, Inc. model 300R ion implanter was used for the implantation work. It allows implantation of positive ionic species at energies from 10 to 300 keV, uniformly over an area 5cm x 5cm. The implanter and its use are described in more detail elsewhere (22).

Computer Programs. Programming was done primarily in FORTRAN and stored on disk for use by the PDP 11/20. The main program IONPIX, described by Fassett, et. al. (23), was used for image pretreatment and preliminary calculations. Two new programs, LTEPIX and MISRPX, were written to perform calculations for the LTE and MISR corrections, respectively.

The LTE correction program, LTEPIX, is written in FORTRAN and is similar in many ways to the IONPIX structure, notably in its scratch file setup. LTEPIX will accept one digitized internal standard file and up to ten unknown element files.

A one-parameter LTE correction routine similar to that used by Rudat and Morrison (16) was the basis for this program. For the sake of familiarity we retain the connotation of "temperature" for the variable parameter T, but make no pretenses of attempting to justify its validity in a thermodynamic sense. The first operation is the generation of a T-parameter map file using the internal standard file and concentration. In this case the internal standard element is assumed to be constant over the entire image. T is incremented in steps of 25K from 4000K to 10,000K (typical values for T-step, T-start, and T-end), and then in steps of 5K for a final determination after the approximate value was determined. An ionization fraction is calculated, the detected signal is corrected to total internal standard atoms sputtered, and this result compared to total atoms sputtered to yield a calculated concentration. In contrast to most LTE corrections which sum the calculated results for all species present, a measurement of the sputtering rate in atoms/second/point is used to determine the total sputtered atoms. This eliminates the need for ion micrographs of all elements present, which is especially helpful in cases where mass interferences or sensitivity problems are present. Sputtering rate was determined by a measurement of the sputtered crater depth using a Rand TALYSTEP stylus measuring device. The crater depth was constant to within 10% from point to point, and was therefore assumed to be constant for this study.

The best T fit is determined in this manner for each point of the image. The completed T-map is then used to calculate concentration maps for all specified unknown element images. Partition functions were calculated for T values up to 10,000K from tables of coefficients published by de Galan, et. al. (24).

The empirical sensitivity factor correction program, MISRPX, is also written in FORTRAN in a format similar to the software previously described. The correction is based on the Matrix Ion Species Ratio (MISR) correction of Gangei, et. al. (7). This method uses a series of sensitivity factor curves generated using an external standard of a similar matrix composition, and requires the knowledge of a reference element concentration in the unknown sample. The MISR correction curves were reduced to discrete values to allow their use in a lookup table format.

The program allows input of two matrix species image files and up to ten unknown image files. The matrix species are ratioed at each point to determine the applicable sensitivity factor for each element. The unknown image files are then corrected to concentration.

Sample. The sample used was NBS SRM-664, a low alloy steel. This steel contains 0.87 weight percent carbon and numerous other elements at certified values ranging from 0.49 weight percent (Mo) down to 0.00007 weight percent (La). The sample was cut and mounted in Sn/Bi eutectic and rough polished with SiC paper down to 600 grit. Further polishing was done with 6-μm alumina to yield a smooth metallurgical finish. All polishing was done using a Buehler, Ltd. 69-1000 Minimet Polisher/Grinder. After polishing, samples were rinsed with acetone, methanol, and isopropanol, and then blown dry.

Procedure. Experimental parameters were as follows. The primary ion beam was oxygen ($O_2^+/O^+ \cong 10$) at an energy of 5.5 keV relative to the sample. An area 400 μm x 400 μm was bombarded at a current density of 6×10^{-4} A/cm^2.

pulse detection mode; images were recorded on electron sensitive film contained within the vacuum system of the ion microscope. Analyses were conducted at residual instrument vacuum (10^{-7} torr). In all cases, detection was of positive secondary ions.

Each digitized ion image is stored as a 256 x 256 point matrix. Each image point has 8-bit resolution (0-255), and represents an area on the sample of about 0.5-0.9 μm^2 in a typical image; thus, none of the 1-μm spatial resolution of the image is lost by the digitization process. Each digitized ion image requires 33K words of magnetic storage.

The sample was ion implanted with PF_3^+ at an energy of 250 keV; the implanted species of interest was ^{19}F. A uniform fluence 3 x 10^{15} atoms/cm^2 was implanted first. Next, a metal mask comprised of horizontal slits 20 micrometers wide and spaced 150 micrometers apart was placed over the sample and it was implanted to a fluence of 2 x 10^{15} atoms/cm^2. Finally, the mask was rotated 90° and a final implant of 4 x 10^{15} atoms/cm^2 was made. The resultant implant was a pattern of crossed stripes of differing concentrations superimposed on a uniform background.

In performing implantation to these concentration levels there is some possibility of sample damage due to sputter errosion of the surface and to radiation damage. The former (on the order of 10 atomic layers) was considered negligable due to the much greater depth of the analysis, and the latter was not observed in this study.

RESULTS

A series of ion images for various constituents of NBS-664 steel was recorded on electron film and digitized via the scanning photodensitometer as described previously. The following discussion will be limited to ^{48}Cr, ^{51}V, and ^{52}Cr, which exhibit no serious mass interferences and span a range of relative heterogeneities within the sample. Images of $^{54}Fe^+$, $^{56}Fe^+$, and $^{56}Fe^+$ were also recorded to serve as internal standards and as matrix ion species for the MISR correction.

In addition, an image of the ^{19}F implant was recorded and digitized. The sensitivity of $^{19}F^+$ was such that the entire implanted region was included in the duration of the exposure. Figure 1 shows a depth profile analysis of the implant. The implant is roughly gaussian in shape, as expected; the mean depth is 290 Å and the standard deviation is 112 Å.

The originally acquired ion images were converted to 256 x 256 point matrices which span 200 μm on the sample surface. Images were registered relative to the $^{56}Fe^+$ image (see reference 15) and a 128 x 128 portion of each image was selected for correction procedures. This eliminated the non-image information present in the original image due to the round format of the film image. Thus, each resultant image file contains 16,384 picture elements (pixels) which correspond to 10,000 μm^2 on the sample surface.

Prior to the application of the two quantification routines some pre-processing of the ion images was required. Images were corrected for the non-linear response of the film (21) and normalized to 1 second exposure times. In addition, images for input to the LTE correction routine were corrected for instrumental discrimination using the factors of Rudat and Morrison (25), for isotopic abundances, and for the non-total coverage of the densitometer.

LTE Correction. LTE correction was first effected using iron as an internal standard, assuming it to be constant in concentration from pixel to pixel. Iron comprises 96.7% of NBS-664. The variable parameter T was searched in steps of 25K from 4000K to 10,000K for the initial approximation, and then in steps of 5K for the final determination. In this way the internal standard ^{56}Fe was fitted to within 0.5% of its certified value at each pixel.

The mean value of T was 7645; T ranged from 6790 to 8155. Images of $^{48}Ti^+$, $^{51}V^+$, $^{52}Cr^+$, and $^{19}F^+$ were then corrected using the value of T which was found for each point of the internal standard image.

A second correction was then done using ^{19}F as the internal standard element. A portion of the fluorine image containing only the uniform background implant was selected for this purpose. Due to the fact that fluorine concentration varied with depth, the total implant was converted to a constant, hypothetical equivalent concentration for calculational purposes (see reference 18). In this case the background implant fluence of 3×10^{15} atoms/cm^2 converted to a mean concentration of 0.024% over the 100 second duration of the $^{19}F^+$ exposure.

Generation of the T-parameter map file for the 128 x 128 pixel internal standard image file required about four hours on the PDP 11/20. This amount of time was necessary since available core memory was insufficient to allow images to be loaded into core in their entirety, necessitating line by line transfers to and from disk storage, and since the T-parameter was searched in steps of 5 to insure a close fit. After the parameter map was complete, correction of each unknown species image required about 10 minutes.

Results of the preceding calculations will be discussed later.

MISR Correction. The matrix ion species ratio correction used the $^{56}Fe_2^+/^{54}Fe^+$ ratio as the basis for calculation of concentrations. The ratio varied from 0.71 to 5.09; the mean was 1.54. The ratio lookup table contained relative sensitivity factors for the unknown elements in intervals corresponding to ratio value spacings of 0.05 from 0.05 to 2.00. Values of $^{56}Fe_2^+/^{54}Fe^+$ between these points were interpolated linearly. Correction required about five minutes for generation of the ratio map and three minutes for correction of each subsequent unknown image.

Sampling. Before discussion of results it is necessary to consider the microsampling situation for the analysis of this sample. As discussed by Drummer, et. al. (26), many of the alloying elements in NBS-664 are present as well defined inclusions. The number and the size and shape distributions of these inclusions are seen to affect the sampling error to be expected from an analysis. The sampling constant method of the above publication makes it possible to estimate sampling error for a bulk analysis of a given size area of the sample. The expected sampling errors for Ti, V, and Cr were calculated by this method, and are 48%, 34%, and 24%, respectively.

DISCUSSION

As a rough approximation of accuracy, the calculated concentrations resulting from both correction schemes were integrated to yield bulk concentrations to facilitate their comparison to the certified values and to each other. The percent relative errors are shown in Table I. Also shown are the certified values and the expected sampling errors.

Results for the LTE calculations shown in Table I are generally within the range of accuracy expected from this type of algorithm (27,28). LTE corrected results are quite often in error by a factor of two or more, but the ability to apply a semi-theoretical approach of this type to a sample with little a priori knowledge other than one internal standard element makes it useful for providing semiquantitative concentration information. (For a more detailed investigation of the relative merits of various semi-theoretical models, see reference 16.)

The MISR corrected results shown in Table I are overall a much closer fit to the certified values, as was anticipated due to the success of this method as applied to bulk-type analyses (7). These results were also very

close to, or within, the ranges of error expected from sampling uncertainties. The apparent success of this analysis as compared to previous sensitivity factor methods is the ability of MISR to compensate for changes in sampling environment by using a varying set of relative sensitivity factors.

Table I also contains the results for the LTE correction using implanted fluorine as an internal standard element, as previously described. It is interesting to compare the results from the different choices of internal standard elements. The fact that there is little overall difference in the accuracies of the calculated concentrations suggests that this method may have potential in providing an internal standard where none otherwise exists. The accuracy of this procedure, of course, as well as the accuracy of the LTE correction for any unknown species in the sample, regardless of the choice of internal standard, is inherently dependent to a large extent on the closeness with which a given element in a particular matrix fits the Saha-Eggert line, which is the basis for the correction. Discretion would therefore be advised in the choice of an element to be implanted for internal standard use, or in the choice of an in-situ internal standard, for that matter.

The LTE correction of the fluorine implant image in Figure 2 is of special interest. Although integration back to bulk concentration can serve as an estimate of accuracy, a successful correction of an image with a known, heterogeneous concentration is more satisfying from an analytical viewpoint. This is especially true since an integrated concentration which differs from the bulk concentration may do so largely due to inhomogeneity of the sample.

In this figure, which has been LTE corrected using iron as an internal standard, the calculated hypothetical equivalent concentrations (18) for various areas of the pattern are compared with the corresponding actual values which were calculated from implantation and analysis parameters. The precisions

of these values result in a precision for the implant concentration of about 10% or better. The calculated values once again compare reasonably to the actual values, considering the accuracy expected of the LTE correction procedure. The primary difference in this particular instance is the ability to evaluate the success of the correction at the point-to-point level rather than comparing results to the bulk concentrations.

A point that we wish to stress is that SIMS in general, and ion microscopy in particular are not bulk-scale techniques, although they are often utilized as such. In many cases it is primarily the fact that a given area or feature may differ from the bulk that is of interest (29,30). Aside from the ability of an ion image analysis to provide semi-quantitative or quantitative results when corrected to concentration, the fact remains that the real power of ion microscopy is to reveal mutli-element, multi-feature characteristics of a sample. In order to do so, it is necessary to examine the data at the individual pixel level. Table 1 is somewhat misleading in that it represents the ion image as a single number; in actuality it contains over 1.6×10^4 information bits - the equivalent of many thousands of 1 micrometer point analyses, collected simultaneously as an image. But even this does not adequately indicate the true value of an imaging analysis, as separate 1 micrometer spots on a sample are seldom of any real interest or great value to the analyst.

A primary objective in using ion microscopy to its full potential is the correlation of structure and composition, which requires the identification of structures within the image field. An important advantage of the ion microscope relative to the ion microprobe is the ability to analyze microfeatures within a recorded image without the presumptive knowledge necessary to allow

correct positioning of the probe, requisite in any probe analysis. The features of interest are composed of groups of interrelated pixels, subsets of the total image. It is this "feature analysis" which exploits the full potential of the ion microscopic analysis.

The first step in feature analysis is the isolation and identification of microstructures of interest. This can be accomplished in a number of different ways, a choice which is usually dependent in part upon the complexity of the feature-field interaction. This problem is not within the scope of this study, but has been investigated by Fassett, et. al. (15).

After the features have been identified, it is possible to calculate relevant descriptors of each feature. Perhaps the most important of these is the concentration of a given species within the feature and as compared to other microstructures within the image field. It is this type of evaluation which comprises the basic philosophy of image feature analysis.

The following is a brief demonstration of the type of morphological compositional information that can be extracted from the previously corrected ion images. It is not our purpose to present an exhaustive treatment, but rather to forward several examples in order to suggest the numerous possibilities of this type of treatment. The following discussion utilizes the MISR corrected images, since in the authors' opinion they are more representative of the true nature of the steel samples analyzed.

The first step is an overall evaluation of the image field to determine the nature and extent of possible microfeatures. One commonly used method of doing this is to view an output of the corrected image in the form of a photographic print or on a CRT display. While some qualitative information is immediately obvious, a disadvantage of this type of display is that any

sort of quantitative evaluation of the features is quite difficult, since perceived brightness (i.e., brightness as perceived by the human visual system) is not a linear function of the light intensity incident on the eye (31). In actual fact, a corrected image displayed in this fashion may not be much more informative than the uncorrected image. The authors feel that the display of results is a matter often given too little emphasis in the presentation of an analysis of this sort, as ineffective display may nullify a great amount of the information gained in correcting the image to concentration space.

An alternate method that we have found to be particularly helpful is the use of three-dimensional representations. Figure 3 shows 3-D plots of the $^{48}Ti^{+}$, $^{51}V^{+}$, and $^{52}Cr^{+}$ images before and after correction to concentration by an LTE calculation using iron as the internal standard. Although absolute numerical values are less accessible in this type of output, the combination of qualitative and quantitative information present makes possible an evaluation of relative sample heterogeneity and concentrations which is often difficult to glean from an intensity-modulated display, in addition to a picture of the spatial relationships of the microfeatures.

These 3-D plots were used to determine parameters for the isolation of features from the image background, as illustrated by the contour plots shown in Figure 4. This method involves delineation of isoconcentration lines by simple thresholding to produce a map which shows areas which lie within given concentration ranges. The crosshatching scheme defined at the bottom allows easy referencing of an area to its corresponding concentration range.

A more in-depth treatment of the titanium image is presented in Figure 5. The feature map locates and labels microfeatures within the image field by thresholding, and

the computer generated image discriptors below it provide additional information, including concentration levels and shape and form factors for each feature. This type of automatic image analysis has been highly developed both scientifically and commercially for the evaluation of microstructures in microscopic fields (32,33) and is quite readily adaptable to ion microscopic analysis.

The preceding examples should suggest to the reader the multitude of possibilities for the applications of digital ion image analysis to materials characterization problems in many disparate fields. The investigations described in this paper only scratch the surface in this dynamic, fast-growing area. The quantification aspect, of course, hinges on the method of quantification of image data. Each of these methods has its particular advantages and pitfalls; each individual analysis situation will dictate the choice of a technique to be used. The use of ion implantation discussed here appears to have a potentially important role to play in some cases where quantification may be otherwise difficult.

Further work to develop image analysis methodology and to extend the scope of ion image feature analysis are presently underway in this laboratory.

ACKNOWLEDGEMENT

The authors are grateful to W. C. Harris and Zhu Dachang for their assistance with the ion implantation work, and to E. Kirkland for his invaluable help with the microphotodensitometer system. The implant facilities of the National Research and Resource Facility for Submicron Structures at Cornell were used.

LITERATURE CITED

1. Heinrich, K. Adv. Opt. Electron Microsc. 1977, 6, 275-301.

2. Yakowitz, H.; Goldstein, J.I. in "Practical Scanning Electron Microscopy", J.I. Goldstein and H. Yakowitz, Ed., Plenum Press, New York, New York 1975, Chapt. II.

3. Liebel, H. J. Appl. Phys. 1967, 38, 5277-5283

4. Williams, P.; Evans, C.A.; Grossbeck, M.L.; Birnbaum, H.K. Anal. Chem. 1976, 48, 964-968.

5. McDonald, N.C. in "Electron Microscopy: Physical Aspects", D. Beaman and B. Siegel, Ed., Wiley, New York, New York 1974, Chapt. 4.

6. Powell, B.D.; Woodruff, D.P.; Griffiths, B.W. J. Phys. E. 1975, 8, 548-552.

7. Ganjei, J.D.; Leta, D.P.; Morrison, G.H. Anal Chem. 1978, 50, 285-290.

8. Yu, M.L.; Reuter, W. Solid State Physics, (#33814, 8/10/79), RC7811.

9. Steiger, W.; Rüdenauer, F.G. Anal. Chem. 1979, 51, 2107-2111.

10. Ganjei, J.D.; Morrison, G.H. Anal. Chem. 1978, 50, 2034-2039.

11. Andersen, C.A.; Hinthorne, J.R. Anal. Chem. 1973, 45, 1421-1438.

12. Schilling, J.H.; Büger, P.A. Int. J. Mass Spectrom & Ion Phys. 1978, 27, 283-290.

13. Kobayashi, H.; Suzuki, K.; Yukawa, K; Tamura, H.; Ishitani, T. Rev. Sci. Instrum. 1977, 48, 1298-1302.

14. Schilling, J.H., Büger, P.A.; Fidos, H. 12th Annual Conference of Microbeam Analysis Society, 1977, Boston, Mass.

15. Fassett, J.D.; Morrison, G.H. Anal. Chem. 1978, 50, 1861-1866.

16. Rudat, M.A.; Morrison, G.H. Anal. Chem. 1979, 51, 1179-1187.

17. Wilson, R.G.; Brewer, G.R. "Ion Beams With Applications To Ion Implantation", Wiley, New York, 1973.

18. Leta, D.P.; Morrison, G.H. Anal. Chem. 1980, 52, 277-280.

19. Castaing, R.; Slodzian, G. J. Microsc. 1962, 1, 395-410.

20. Morrison, G.H.; Slodzian, G. Anal. Chem. 1975, 47, 932A-943A.

21. Fassett, J.D.; Roth, F.R.; Morrison, G.H., Anal. Chem. 1977, 49, 2322-2329.

22. Leta, D.P., Ph.D. Thesis, Cornell University, Ithaca, New York 1979, Chapter 2.

23. Fassett, J.D.; Drummer, D.M.; Morrison, G.H. Anal. Chim. Acta (Computer Techniques and Optimization) 1979, 112, 165-173

24. deGalan, L.; Smith, R., Winefordner, J.D. Spectrochim. Acta 1968, Part B, 23, 521-525.

25. Rudat, M.A.; Morrison, G.H. Int. J. Mass Spectrom. & Ion Phys. 1978, 27, 249-261.

26. Drummer, D.M.; Fassett, J.D.; Morrison, G.H. Anal. Chim. Acta 1978, 100, 15-22.

27. Morgan, A.E.; Werner, H.W. Mikrochim. Acta 1978, II, 31-50.

28. Simons, D.S.; Baker, J.E.; Evans, C.A. Anal. Chem. 1976, 48, 1341-1347.

29. Campbell, N.A.; Stika, K.M.; Morrison, G.H. Science 1979, 204, 185-187.

30. Walsh, J.M., Kear, B.H. Metallurgical Transactions A 1975, 6A, 226-229.

31. Gonzalez, R.C.; Wintz, P. "Digital Image Processing", Addison-Wesley, Reading, Mass., 1977, Chapter 2.

32. Nazaré, S.; Ondracek, G. Microscope 1974, 22, 39-58.

33. Underwood, E.E. Microscope 1974, 22, 69-80.

CREDIT

This work was funded by the National Science Foundation, the Office of Naval Research, and the Cornell Materials Science Center.

Table I. LTE and MISR Corrected Results for NBS SRM-664

Element	Certified Concentration	Relative Error[a] LTE(Fe)[b]	LTE(F)[b]	MISR	Expected Sampling Error
Ti	0.24%	-109%	-156%	-30%	48%
V	0.10%	+77%	+40%	+46%	34%
Cr	0.06%	-50%	-22%	0%	24%

a. Integrated image area compared to certified bulk concentration

b. Internal standard element

CAPTIONS

Figure 1. Depth profile analysis of ^{19}F implanted into NBS SRM-664.

Figure 2. LTE corrected fluroine implant image showing average concentration for labelled areas.

(1) 0.044%: + 83% relative error

(2) 0.070%: + 75% relative error

(3) 0.105%: + 88% relative error

(4) 0.130%: + 81% relative error

Figure 3. (a), (c), (e) Uncorrected 3-D plots of $^{48}Ti^+$, $^{51}V^+$, and $^{52}Cr^+$ in NBS SRM-664 steel; (b), (d), (f) Corrected plots of $^{48}Ti^+$, $^{51}V^+$, and $^{52}Cr^+$. Field of view is 100 micrometers.

Figure 4. Isoconcentration contour plots of (a) $^{48}Ti^+$, $^{51}V^+$, (c) $^{52}Cr^+$ in NBS SRM-664, corrected to concentration by LTE calculation using Fe as an internal standard. Concentration ranges in percent defined below each plot. Field of view is 100 micrometers.

Figure 5. (a) Feature map of $^{48}Ti^+$ image for a different sampled area of NBS SRM-664. Field of view is 100 micrometers.

(b) Feature descriptors of number features. LABEL - feature number; AREA - number of pixels in feature; TOTP - number of perimeter points; EP - number of points on edge of image; FF1 - form factor (see ref. 32,33); IYT, IYB, IXL, IXR - coordinates of feature limiting boundaries; FF2 - form factor; AVGI - average intensity (concentration) of feature; SD - standard deviation within feature.

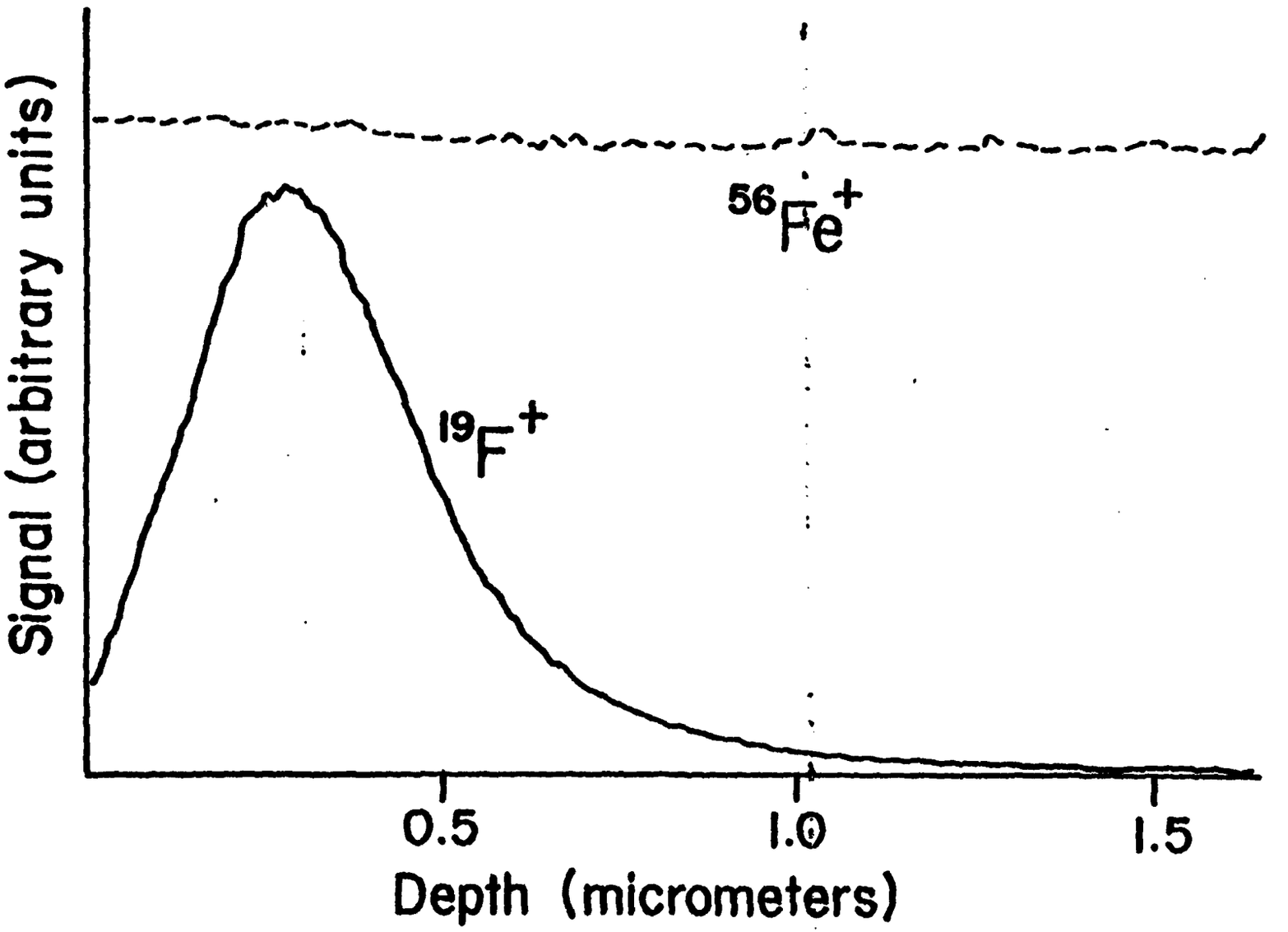

Figure 1

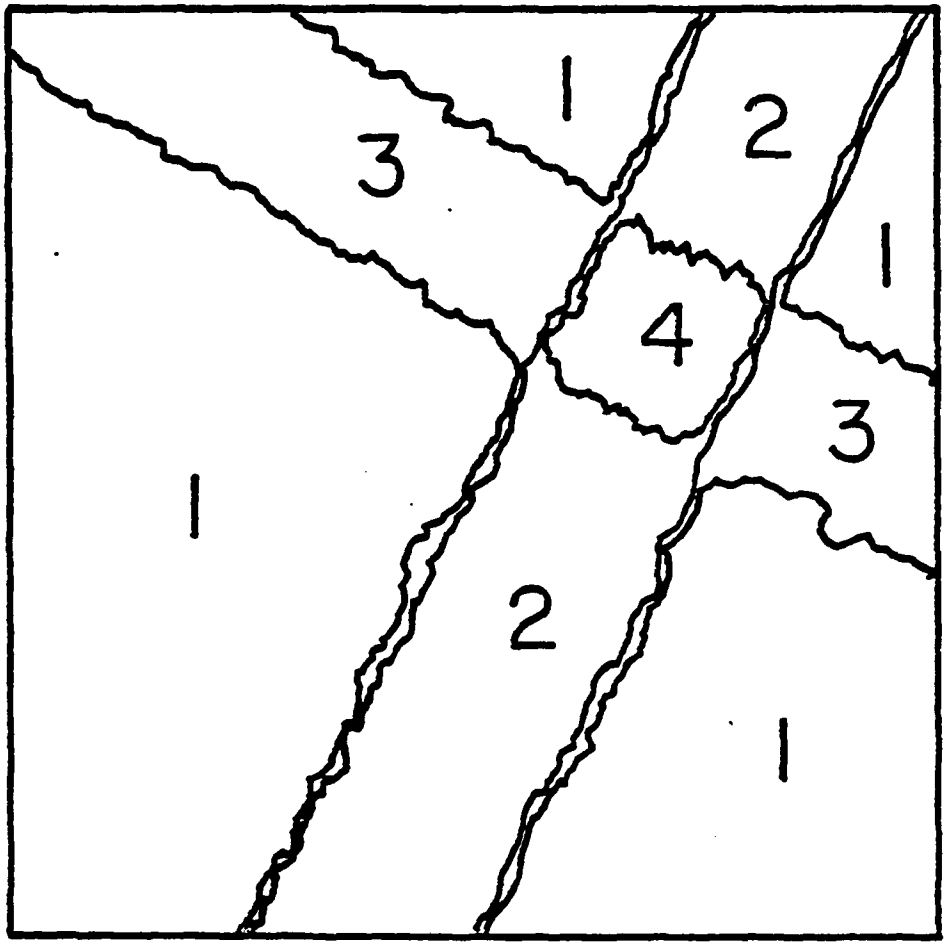

FIGURE 2

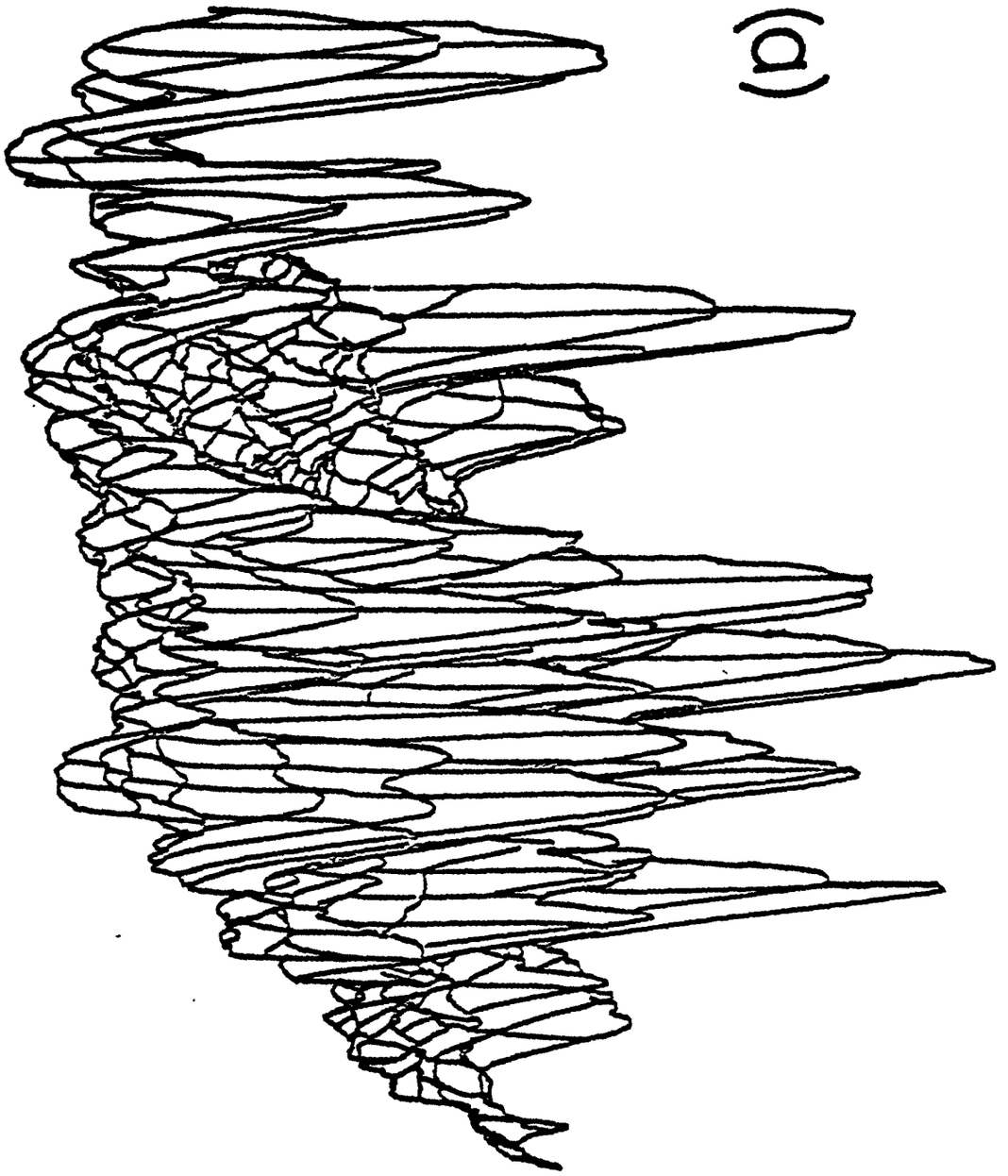

FIG. 3a

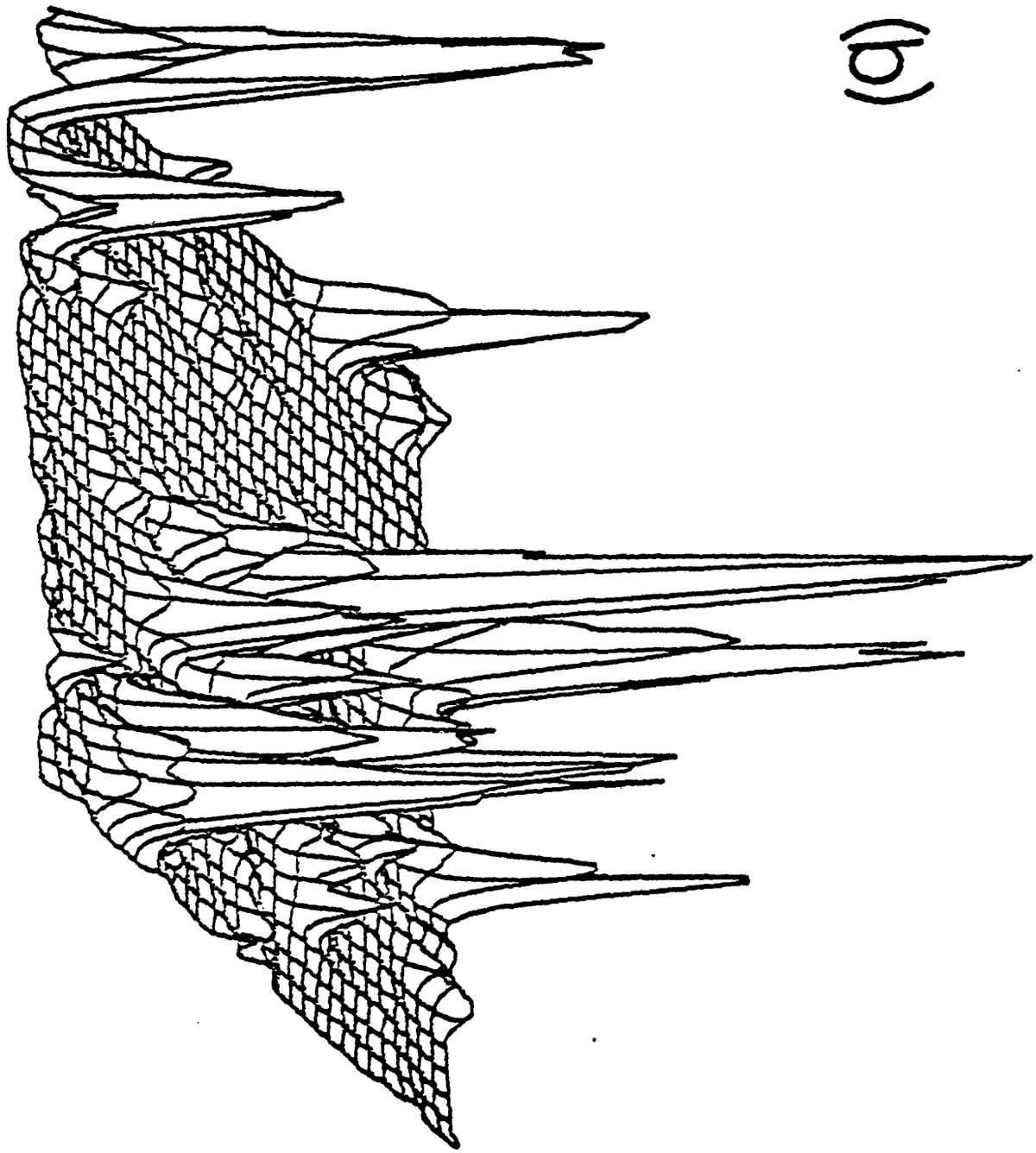

Figure 3b

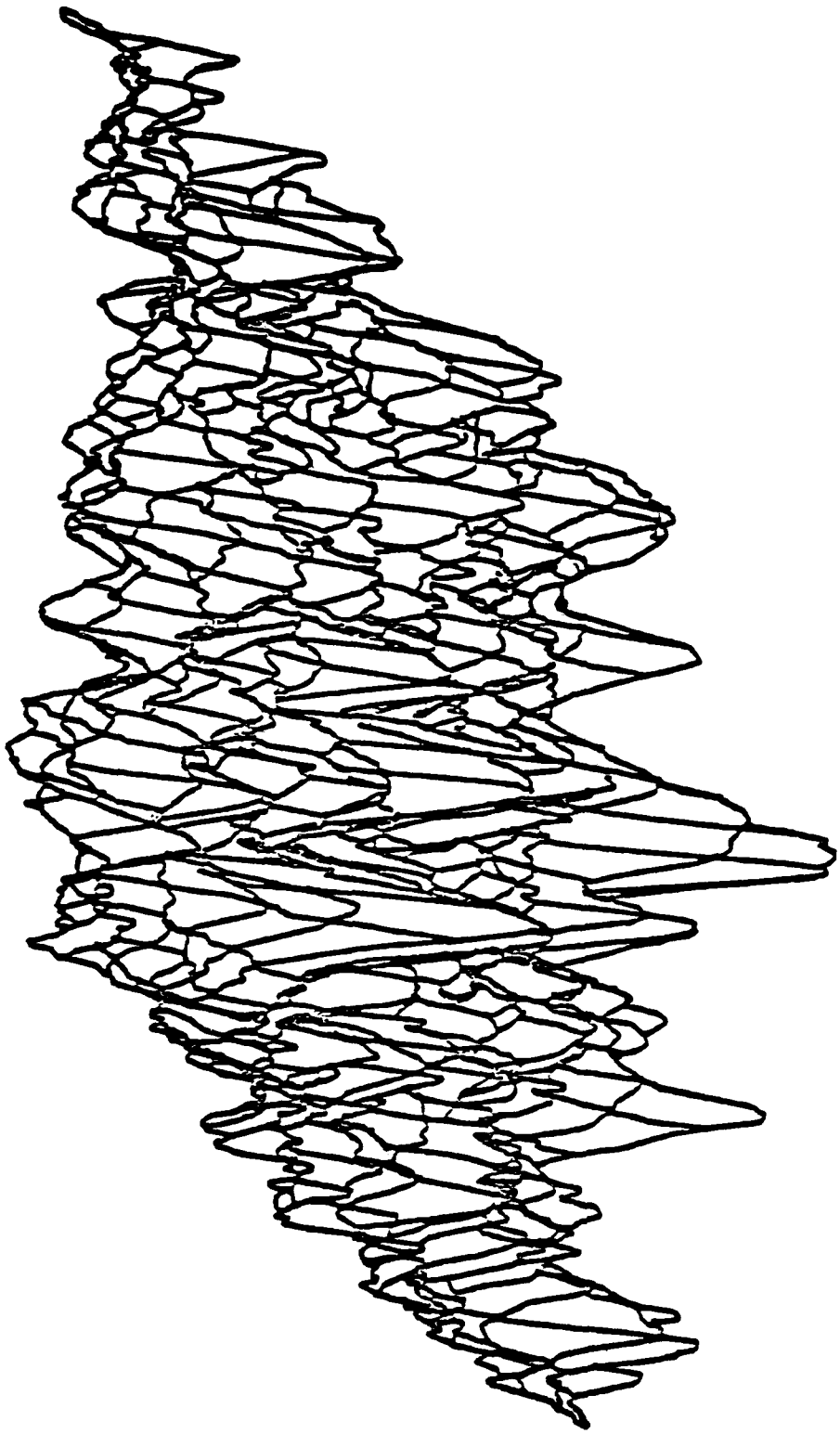

(c)

Figure 3c

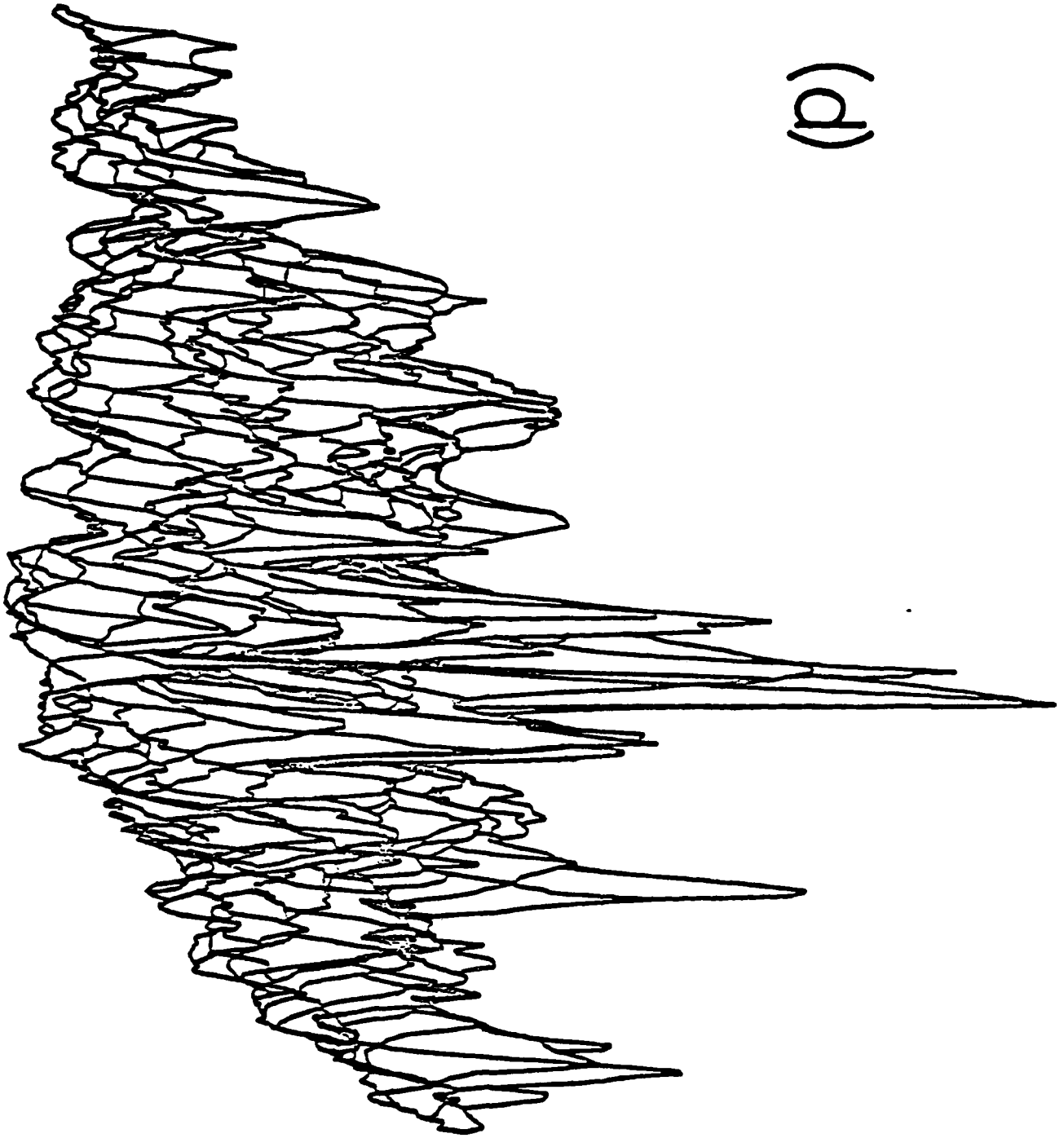

Figure 3d

(a)

Figure 3a

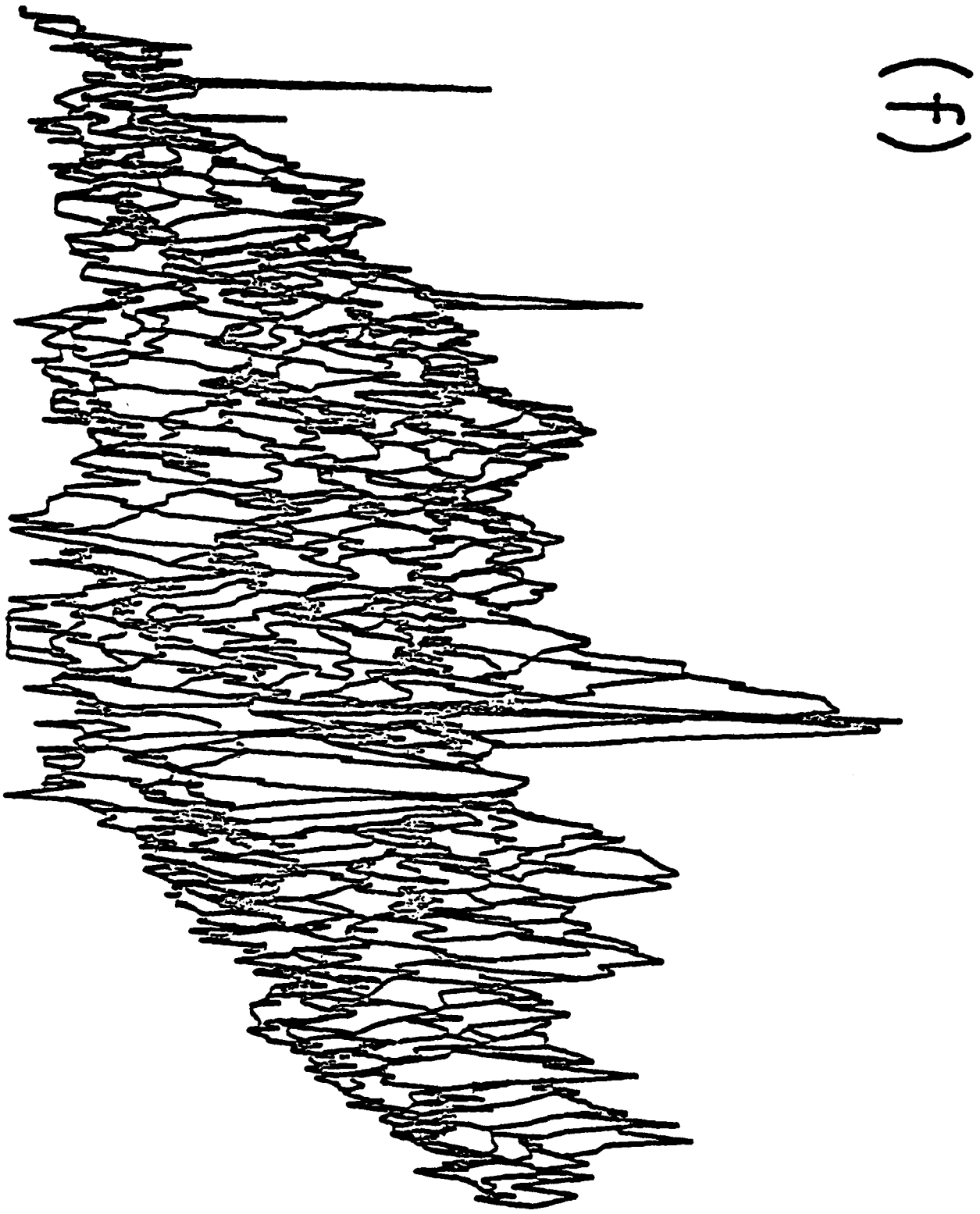

Figure 3F

(a)

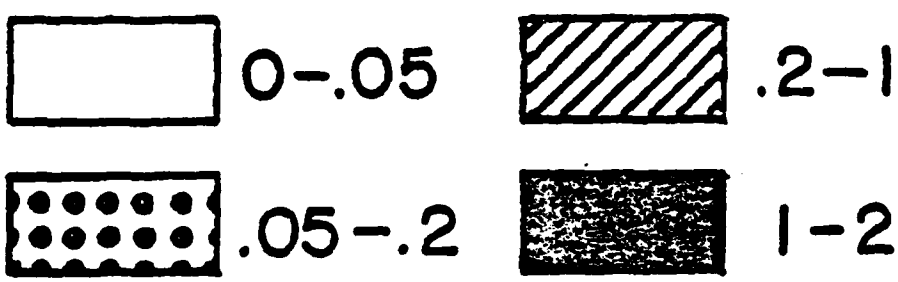

(b)

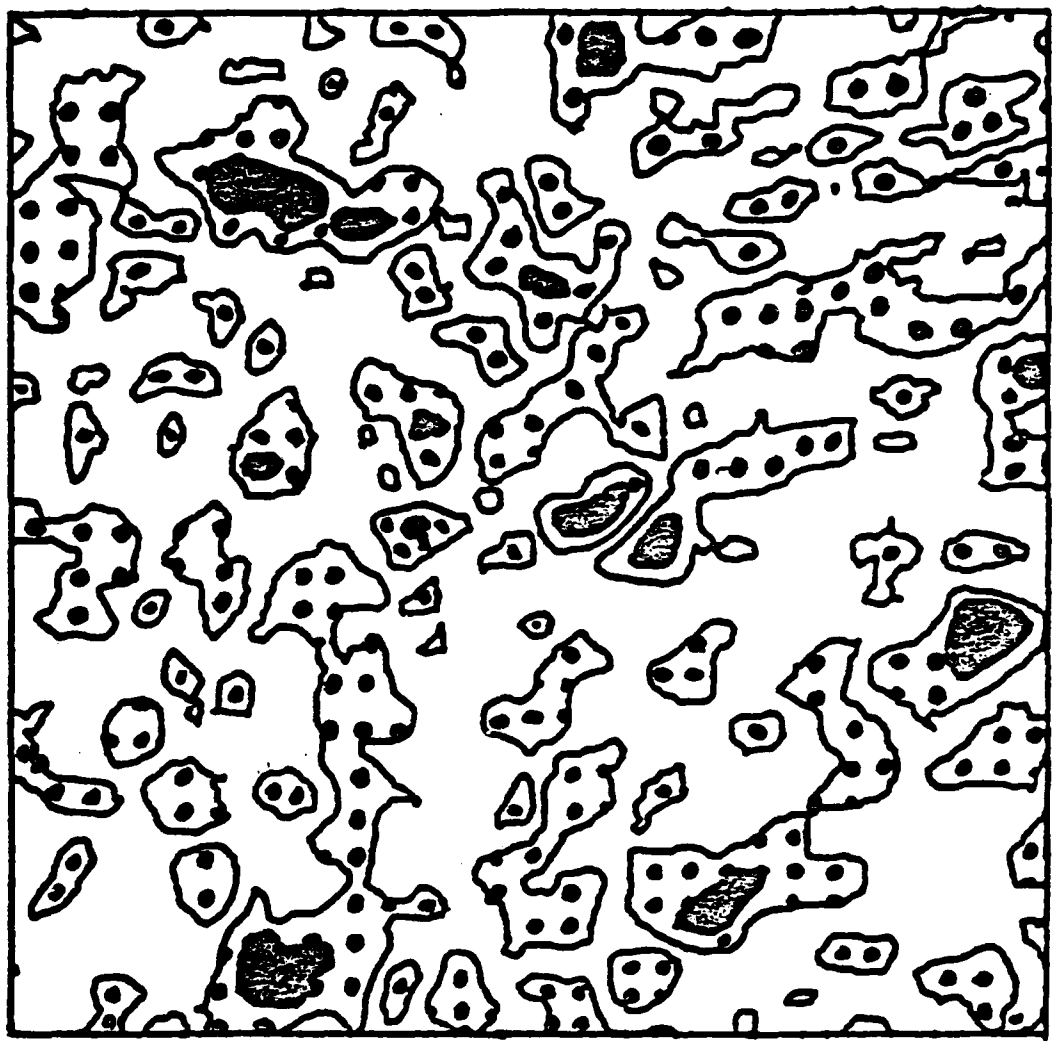

0–.05

.1–.2

.05–.1

Figure 46

(C)

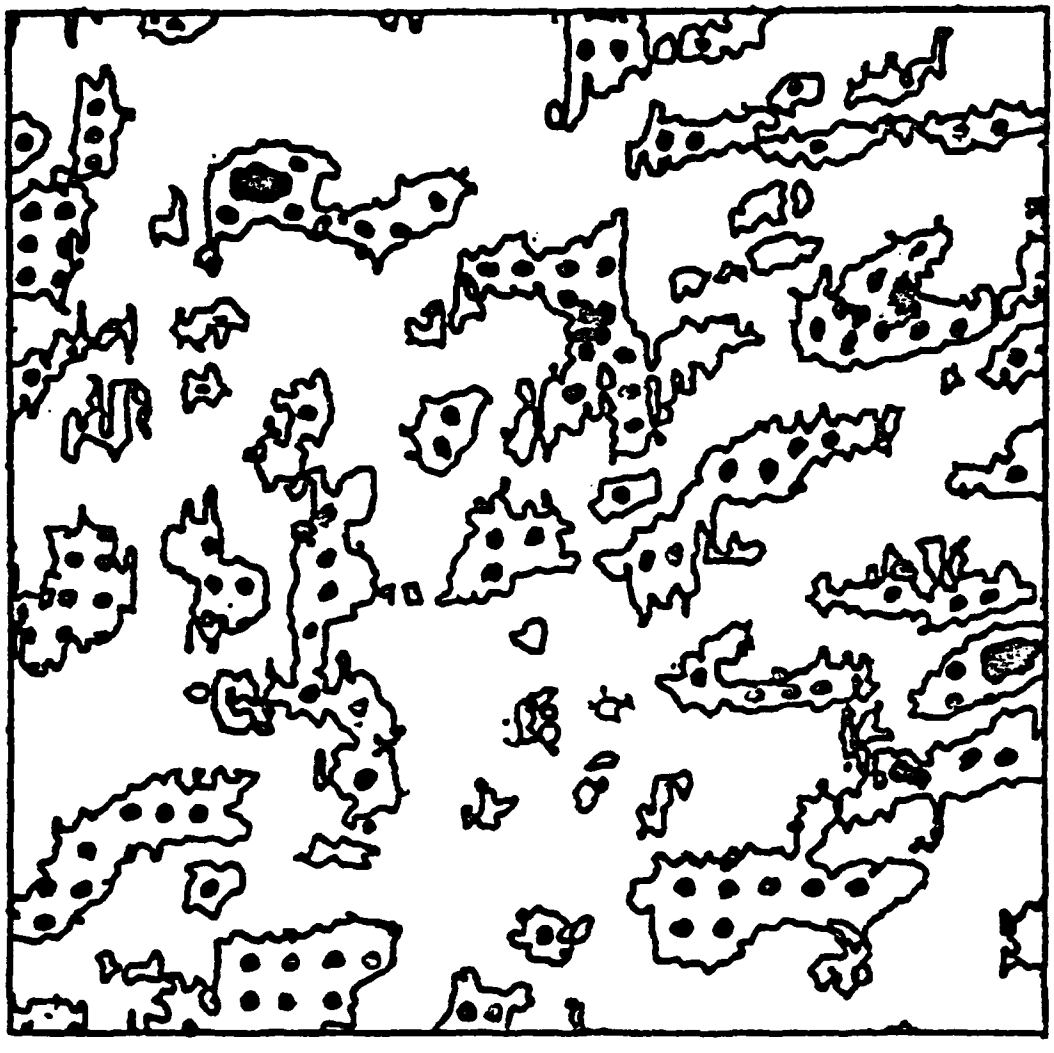

0–.02

.05–.1

.02–.05

Figure 5a

(b)

LABEL	AREA	TOTP	EP	FF1	IYT	IYB	IXL	IXR	FF2	AVG1	SD
1	171	58	20	0.8133	1	14	1	15	1.071	1.709	1.313
2	229	96	8	0.3976	1	24	18	36	0.792	0.6701	0.5423
3	51	36	2	0.6296	1	9	98	106	1.000	0.3466	0.1232
4	6	12	0	0.6667	12	14	37	39	1.000	0.2160	0.1099E-01
5	386	114	0	0.4752	16	40	98	122	1.000	0.9900	0.7977
6	23	22	0	0.7603	26	32	31	34	0.571	0.2609	0.4211E-01
7	17	22	0	0.5620	26	32	64	66	0.429	0.2280	0.1863E-01
8	1	4	0	1.0000	26	26	97	97	1.000	0.3725	0.3725
9	260	110	0	0.3438	33	63	73	91	0.613	0.6191	0.4374
10	308	112	0	0.3929	42	77	57	71	0.417	1.211	1.448
11	6	14	6	0.4098	52	57	1	1	0.167	0.3662	0.6020E-01
12	18	23	7	0.5950	55	61	125	128	0.571	0.4578	0.2531
13	5	10	0	0.8000	64	66	119	120	0.667	0.2114	0.7606E-02
14	1	4	0	1.0000	65	65	126	126	1.000	0.2149	0.2149
15	111	56	0	0.5663	72	85	89	92	0.929	0.9731	0.7433
16	98	68	0	0.3391	74	87	96	109	1.000	0.3608	0.1182
17	44	32	0	0.6875	86	95	43	48	0.600	0.3156	0.6777E-01
18	118	54	10	0.6475	94	110	1	10	0.500	0.9457	0.6540
19	34	30	0	0.6044	96	104	85	90	0.667	0.3532	0.1166
20	227	98	0	0.3782	103	125	44	63	0.870	0.9097	1.019
21	8	14	0	0.6531	111	115	126	127	0.400	0.2410	0.2564E-01
22	39	32	0	0.6094	115	121	5	13	1.286	0.2437	0.3075E-01
23	88	44	6	0.7273	116	128	79	88	0.769	0.8060	0.6357
24	36	42	5	0.3265	116	128	99	107	0.692	0.2799	0.1040
25	18	20	3	0.7200	122	128	7	10	0.571	0.2429	0.3080E-01
26	4	4	1	4.0000	127	128	95	97	1.500	0.2513	0.3562E-01

Figure 5b